Journal of Power Sources, 25 (1989) 215 - 227

POWER LOSSES IN BATTERIES WITH A COMMON ELECTROLYTIC PATH

C. J. GABRIEL and S. SZPAK*

Naval Ocean Systems Center, San Diego, CA 92152-5000 (U.S.A.)

(Received April 22, 1988; in revised form November 21, 1988)

Summary

The distribution of power losses in an operating electrochemical power source of pile construction provided with a common manifold is discussed. The developed relationships yield information that can guide the battery design to meet *a priori* specified requirements. Selected illustrative examples pertain to the Li/$SOCl_2$ system.

Introduction

Two types of designs for high-power-output, energy-dense, electrochemical systems are under active development: (i) the flowing electrolyte and (ii) the static electrolyte, reserve type, thin cell approach. Both designs utilize a modular concept and both have a common manifold which provides the means for maintaining forced flow of the electrolyte or activating the battery.

In the course of an assessment of the battery operational capabilities, information on power output and efficiency are often required. Calculations yielding this information are relatively simple for single cells or batteries without a common electrolytic path, but they are more difficult when a common manifold is employed. In such designs, the optimization procedure must consider all losses, including those attributed to the intercell currents, a consideration only rarely treated in the literature [1].

This communication examines only the effect of intercell currents on the power density and efficiency of an operating electrochemical system. The method is general — the examples to illustrate the selected points pertain to the Li/$SOCl_2$ batteries. The assumptions underlying the treatment are identical with those used in ref. 2.

General consideration

An electrochemical cell is a constrained system that reacts spontaneously as the constraints are removed. In principle, the removal of constraints, *i.e.*,

*Author to whom correspondence should be addressed.

Elsevier Sequoia/Printed in The Netherlands

the cell discharge, can be carried out reversibly; in practice, however, irreversible processes do occur, thus reducing the extractable energy content. As a rule, the analysis of energy conversion is performed under restrictive conditions of a constant pressure and temperature. Under these conditions, by combining the first and second laws of thermodynamics, eqns. (1) and (1a) hold for a single cell

$$(U - V)J_1 = T \sum_{k=1}^{K} (\mathrm{d}_i S)_k \tag{1}$$

or

$$(U - V)J_1 = J_1^2 R_z \tag{1a}$$

where terms on the right side of eqns. (1) and (1a) account for the rate of heat generation by the K irreversible processes associated with the flow of current, J_1. As written, R_z in eqn. (1a) is the cell internal impedance, *i.e.*, it includes losses due to anodic and cathodic overpotentials (ref. 2, eqns. (11) and (13)). Consequently, eqn. (1) is the basis for the examination of the effect of intercell currents on both the power delivered to the load and the cell/battery efficiency. Furthermore, as written, eqn. (1) states that the difference between the cell/battery own power and that delivered to the load appears in the form of Clausius uncompensated heat, which must be removed to maintain constant temperature [3]. Here, the battery own power is equivalent to the power of irreversibility, as defined by van Rysselberghe [4]. Moreover, for a single cell, or in the absence of intercell currents, eqn. (2) applies

$$I_{c,n} = I_{a,n} = J_1 \tag{2}$$

because the electrode currents, $I_{a,n}$ and $I_{c,n}$, are also equal to the load current, J_1.

From Fig. 1, where the potential distribution across the discharging cell is schematically illustrated, we have

$$U = U_c - U_a \tag{3}$$

and

$$V = V_c - V_a \tag{3a}$$

Substitution of eqns. (2) and (3) into eqn. (1) yields, after rearrangement, eqn. (4)

$$(U_c I_c - U_a I_a) - (V_c I_c - V_a I_a) = T \sum_{k=1}^{K} (\mathrm{d}_i S)_k \tag{4}$$

Identifying the first term in eqn. (4) as the cell own power, P_b, and the second term as the power into the load, P_1, we can now examine the effect of the presence of intercell current, I_n, on the power output as well as cell/battery efficiency through the relationship, eqn. (5), see Fig. 2.

$$I_{c,n} = I_n + I_{a,n} \tag{5}$$

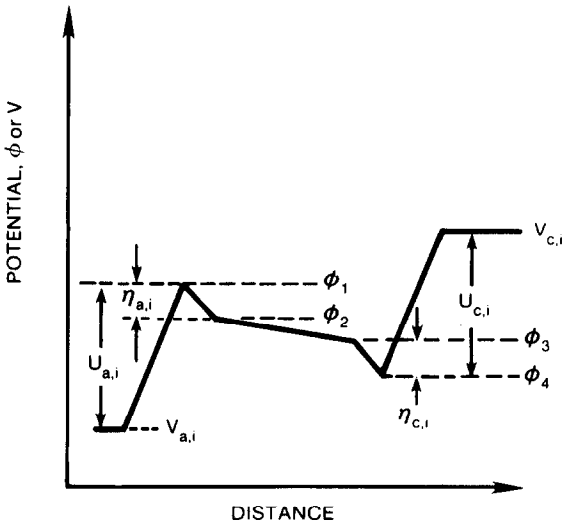

Fig. 1. Idealized distribution of electric potential within a cell, where the sign conventions used here for $U_{a,c}$ and $\eta_{a,c}$ are defined by: $U_a = V_a - \Phi_1$, $U_c = V_c - \Phi_4$; $\eta_a = \Phi_1 - \Phi_2$; $\eta_c = \Phi_3 - \Phi_4$; $J_1 R_z = \Phi_2 - \Phi_3$.

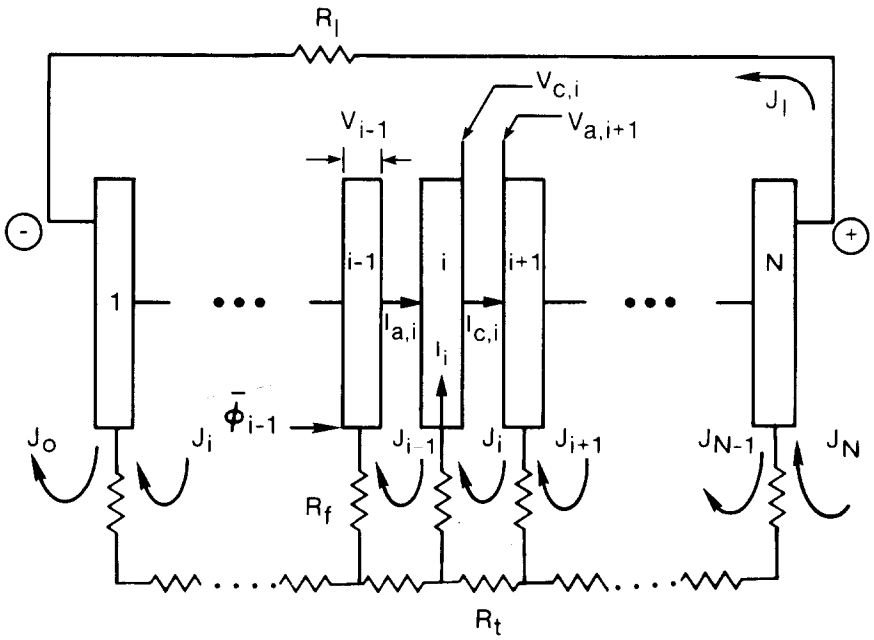

Fig. 2. Module representation by electric circuit analog. V_{i-1}, cell voltage; Φ_{i-1}, potential at inlet to $(i-1)$th cell; $I_{a,i}$, $I_{c,i}$ and I_i, anode, cathode and intercell current, respectively; J_i, circulating current; J_l, loop current in external resistor, R_l; R_f, manifold feed-line resistor; R_t, equivalent fill tube resistor.

However, the right hand side of the generalization of eqn. (4) will no longer have the simple dependence on J_1 indicated in eqn. (1a), because it must include losses in the manifold as well as losses within cells themselves generated by intercell currents.

Power losses

Limiting the discussion to losses associated with the presence of a common electrolytic path, we have, for the arrangement shown in Fig. 2, the battery own power and the power delivered to the load, given by the relationships, eqns. (6) and (6a), respectively

$$P_b = \sum_{n=1}^{N} (U_{c,n} I_{c,n} - U_{a,n} I_{a,n}) \tag{6}$$

and

$$P_l = \sum_{n=1}^{N} (V_{c,n} I_{c,n} - V_{a,n} I_{a,n}) \tag{6a}$$

In the case of a battery employing identical cells with constant parameters, using relationships derived previously [2], *viz.*

$$\sum_{n=1}^{N} I_n = 0$$

and

$$\sum_{n=1}^{N} I_{a,n} = NJ_1 + \sum_{n=1}^{N} J_n$$

eqns. (6) and (6a) become eqns. (7) and (7a)

$$P_b = U\left(NJ_1 + \sum_{n=1}^{N} J_n\right) \tag{7}$$

and

$$P_l = J_1 \sum_{n=1}^{N} V_n \tag{7a}$$

Using eqn. (8)

$$\sum_{n=1}^{N} J_n = \frac{NU - J_1(R_1 + NR_z)}{R_z} \tag{8}$$

and expressing J_1 in terms of battery voltage and design parameters, ref. 2, eqn. (28), we obtain

$$P_b = \frac{NU^2}{R_z}\left[\frac{N(1-\zeta)R_z + R_1\zeta}{N(1-\zeta)R_z + R_1}\right] \tag{9}$$

Similarly, using the relationship

$$\sum_{n=1}^{N} V_n = R_l J_l$$

we have for the power delivered to the load, eqn. (10)

$$P_l = \left[\frac{N(1-\zeta)U}{R_l + N(1-\zeta)R_z}\right]^2 R_l \tag{10}$$

The battery power consumed in all processes, including the presence of intercell currents, is obtained upon subtracting eqn. (10) from eqn. (9). The result in a dimensionless form is given by eqn. (11)

$$\Pi = \frac{1-\zeta+\zeta\rho}{1-\zeta+\rho} - \rho\left[\frac{1-\zeta}{1-\zeta+\rho}\right]^2 \tag{11}$$

where the two terms on the right are dimensionless powers, $\Pi_\alpha = R_z P_\alpha / NU^2$ with α = b, l, respectively, and the dimensionless resistance $\rho = R_l/NR_z$.

The parameter ζ, appearing in eqns. (9) - (11), is related to the battery design as well as to the electrochemical system employed [2]. This relationship is given by eqn. (12)

$$\zeta = \frac{R_z}{R_t + R_z}\left[1 - \frac{(\lambda^N - 1)(\lambda + 1)}{N(\lambda^N + 1)(\lambda - 1)}\right] \tag{12}$$

where

$$\lambda = 1 + \frac{R_t + R_z}{2R_f^*} + \left[\frac{R_t + R_z}{2R_f^*}\left(2 + \frac{R_t + R_z}{2R_f^*}\right)\right]^{1/2} \tag{12a}$$

and

$$R_f^* = R_f + R_p - R_z\left(\frac{\sigma^2}{\sigma_a \sigma_c}\right) \tag{12b}$$

The respective resistances are identified in Fig. 2 except for the R_p which is the distributed resistance at the port entrance of the cell.

A plot of the dimensionless quantities Π_α as a function of log ρ, eqns. (9) and (10), is shown in Fig. 3. Evidently, the power into the load exhibits a maximum at $\rho = 1 - \zeta$, while the battery own power decreases monotonically with an increasing ρ and, in the limit, as $\rho \to \infty$, $\Pi_b \to \zeta$.

Equation (11), the measure of all losses associated with the battery operation, including those due to the presence of the common electrolytic path, can be examined with the aid of Fig. 3. For a given ζ, this power consumption, $\Pi_b - \Pi_l$ increases from ζ to 1 with decreasing ρ. For ρ less

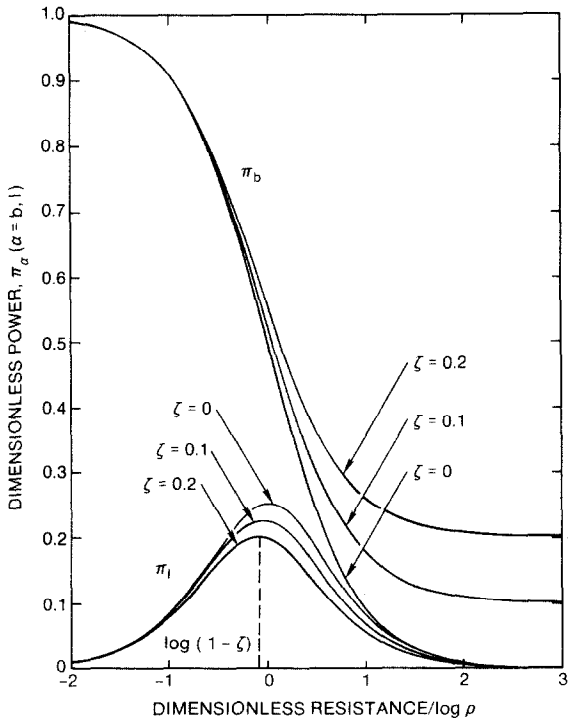

Fig. 3. Plot of dimensionless power, Π_α, with α = l, b as a function of dimensionless resistance, ρ, for ζ = 0, 0.1 and 0.2, as indicated.

than $1 - \zeta$, it increases rapidly becoming, in effect, independent of whether or not a common electrolytic path is maintained.

Distribution of power losses

The distribution of power losses can be conveniently examined with the aid of eqns. (4), (6) and (6a). Considering Fig. 2, the total losses are separated into their components by an assumed electric circuit analog; in eqn. (4) these losses are expressed by the term

$$T \sum_{k=1}^{K} (\mathrm{d}_i S)_k$$

We can now identify:

(i) losses occurring within the cells, with or without intercell currents present, eqn. (13);

(ii) losses in the manifold tube, eqn. (14);

(iii) losses in the feed lines, eqn. (15)

$$P_z = P_b - P_l - P_t - P_f \qquad (13)$$

where

$$P_t = R_t \sum_{i=1}^{N} J_i^2 \tag{14}$$

and

$$P_f = \sum_{i=1}^{N} I_i^2 R_{f,i} \tag{15}$$

When there are no intercell currents, eqn. (2) holds and, under the conditions leading to eqn. (1), eqn. (13) would become eqn. (16)

$$P_z = J_1^2 \sum_{i=1}^{N} R_{z,i} \tag{16}$$

This equation, along with eqns. (14) and (15), would then provide the cell-to-cell distribution of power losses, because each term in these equations can be assigned to a particular location in the battery. However, in the presence of intercell currents, the total power loss specified by eqn. (13) cannot be distributed among the cells without additional assumptions. These assumptions are required by the application of the trapezoidal rule to certain integrals in the model of ref. 2, eqns. (A-4) - (A-7). Consequently, the intercell currents, I_i, in eqn. (15) consider only the current and conductivity distribution on the electrodes and not the details of the complicated current and conductivity distributions that actually exist in the region near the entrance port.

The results of a sample calculation using the data from Table 1, ref. 2, applied to a 40-cell $Li/SOCl_2$ battery being discharged through an external load of 20 Ω with the load current J_1 = 6.727 A, are given in Table 1. In this example, the total unaccounted power loss of 1.3 W, which is attributed to the intercell current flow into the cells, is a small fraction of the total power loss. The difference between eqns. (13) and (16) cannot be calculated with the present model for a particular cell; furthermore, in situations where the intercell currents are large, eqn. (16) should not be used.

Experience shows that often in the course of the discharging of an $Li/SOCl_2$ battery, in addition to normal changes taking place within a cell, dendritic Li growths appear in the feed lines at the negative end of the battery and corrosion damage is found localized at the positive end [2]. The dendritic growth occurring in the feed lines reduces resistance in the electrolyte, causing a shift in the distribution of intercell and circulating currents (ref. 2, Fig. 9). This shift affects both the profile and the magnitude of the dissipative processes in the manifold. An example of this time dependence, calculated as in ref. 2, for the above 40 cell battery, is shown in Fig. 4 where the profiles of the power dissipation in the manifold at τ = 0, τ = 0.15, and near the end of cell lifetime, *i.e.*, at τ = 0.9, Fig. 4(a), (b) and (c), respectively, are displayed. It is seen that at τ = 0, this profile is symmetrical with the maximum dissipation occurring at the battery ends and showing minima at the 5th and 35th cells. With the passage of time, however, the

TABLE 1

Power dissipation in a 40 cell $Li/SOCl_2$ module*
(Input data, ref. 2, Table 1.)

Design parameters		
$\lambda = 1.159$		
$\zeta = 7.236 \times 10^{-4}$		
$\rho = 14.36$		
$R_z = 3.482 \times 10^{-2}\ \Omega$		
$R_t = 31.83\ \Omega$		
$R_f = 1457\ \Omega$		
$R_f^* = 1463\ \Omega$		
Power distribution		
Battery own power	P_b, eqn. (9)	987.7 W
Power into load	P_l, eqn. (10)	905.0 W
Power into manifold tube	P_m, eqn. (14)	7.096 W
Power into feedlines	P_f, eqn. (15)	2.302 W
Power dissipated within a cell	P_z, eqn. (16)	63.03 W
Unaccounted power**		3.32×10^{-2} W/cell

*Data from Table 1, ref. 2, used in this calculation.
**Difference between P_z calculated from eqn. (13) and eqn. (16).

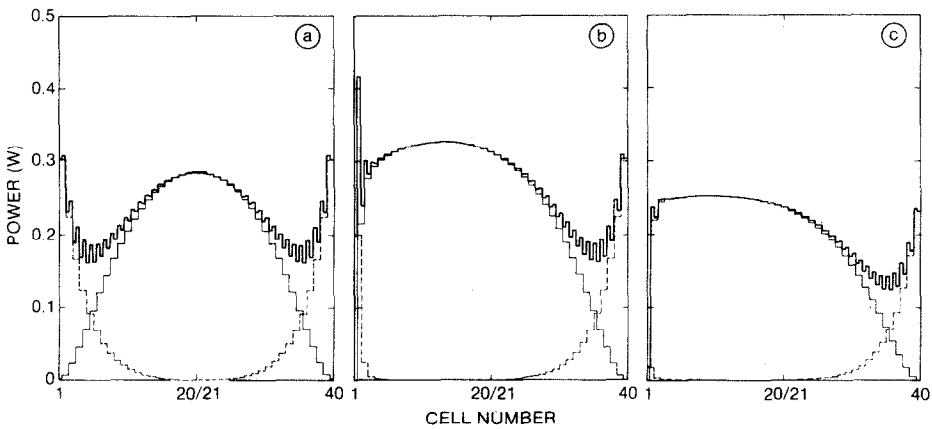

Fig. 4. Distribution of power losses in a 40 cell module, with a 20 Ω load. (a) at $\tau = 0$; $J_l = 6.727$ A; $P_b = 978.7$ W; $P_z = 64.36$ W; $P_l = 905.0$ W. (b) at $\tau = 0.15$; $J_l = 6.701$ A; $P_b = 819.2$ W; $P_z = 67.75$ W; $P_l = 898.1$ W. (c) at $\tau = 0.9$; $J_l = 5.804$ A; $P_b = 846.3$ W; $P_z = 164.2$ W; $P_l = 673.6$ W; P_z calculated from eqn. (13); P_f, dashed lines; P_t, light solid lines; $P_f + P_t$, heavy solid lines.

distribution of the dissipative processes shifts toward the battery negative end and increases somewhat in magnitude because of the increased dissipation in the manifold tube. Very small changes are observed at the positive

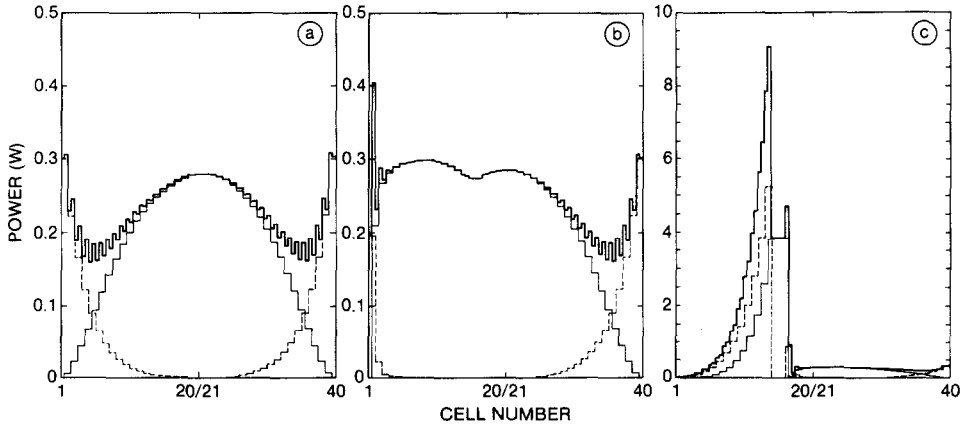

Fig. 5. Discharge time dependent distribution of power losses in a 40 cell module with a 20 Ω load and having defective central cells. (a) at $\tau = 0$; $J_l = 6.685$ A; $P_b = 972.7$ W; $P_z = 69.56$ W; $P_l = 893.9$ W. (b) at $\tau = 0.15$; $J_l = 6.509$ A; $P_b = 948.9$ W; $P_z = 91.21$ W; $P_l = 847.2$ W. (c) at $\tau = 0.3$; $J_l = 0.3472$ A; $P_b = 47.83$ W; $P_z = 1.251$ W; $P_l = 2.412$ W. Deficiency factor $w = 0.2$ for cells 14, 15 and 16; P_z calculated from eqn. (13); P_f, dashed line; P_t, light solid line; $P_f + P_t$, heavy solid line.

end. At the end of the discharge, *i.e.*, at $\tau > 1$, not shown, the residual dissipative losses become small.

Another example of a manifold power loss profile is illustrated in Fig. 5. In this example, it is assumed that in the 40 cell module, the 14th, 15th and 16th cells are defective, with $w = 0.2$. Here, w denotes the computational deficiency factor introduced to account for cell component variation [2]. It is seen that a defective cell or a series of such cells, can cause a concentration of dissipative processes and, therefore, produce a localized heat source of a substantial magnitude. Obviously, creation of such heat sources is undesirable because they may lead to catastrophic events [5].

Condition for trade-off between the P_l and extractable energy

As shown in Fig. 3, in the absence of intercell currents, $\zeta = 0$, the maximum power delivered to the load occurs when $\rho = 1$, *i.e.*, when the battery internal resistance equals the external load, $R_l = NR_z$. Under this condition, half of the stored energy is delivered to the load. In the presence of intercell currents, the maximum power is realized when $\rho = 1 - \zeta$, with only the fraction, $(1 - \zeta)/2(1 + \zeta)$, of the stored energy delivered to the load.

In practice, it is often desired to discharge a battery under conditions that maximize the use of stored energy. These conditions are summarized in Fig. 6 where it is seen that in the absence of intercell currents, the load ρ should be as large as practical since the ratio P_l/P_c increases monotonically with ρ. However, with intercell currents present, this ratio has a maximum when $\rho = (1 - \zeta)\zeta^{-1/2}$. As ρ increases beyond this point, the power dissipation

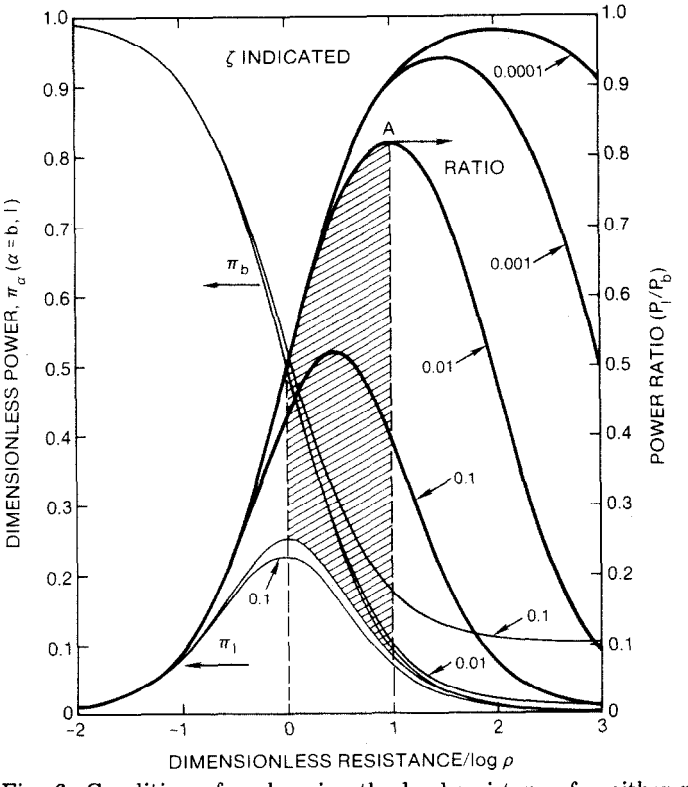

Fig. 6. Conditions for choosing the load resistance for either maximum P_l or minimum battery power dissipation. Point A, max P_l/P_b for $\zeta = 0.01$. Shaded area indicates the region of ρ where an inverse relation exists between P_l and P_l/P_b for $\zeta = 0.01$.

TABLE 2

Values of dimensionless quantities at the trade-off limits

ρ	$1-\zeta$	$(1-\zeta)\zeta^{-1/2}$
$\frac{P_l}{P_b}$	$\frac{1-\zeta}{2(1+\zeta)}$	$\frac{1-\zeta^{1/2}}{1+\zeta^{1/2}}$
Π_l	$\frac{1-\zeta}{4}$	$\zeta^{1/2}\frac{(1-\zeta^{1/2})}{1+\zeta^{1/2}}$
Π_b	$\frac{1+\zeta}{2}$	$\zeta^{1/2}$
L_M	2ζ	$\frac{2\zeta^{1/2}}{1+\zeta^{1/2}}$
L_P	ζ	—

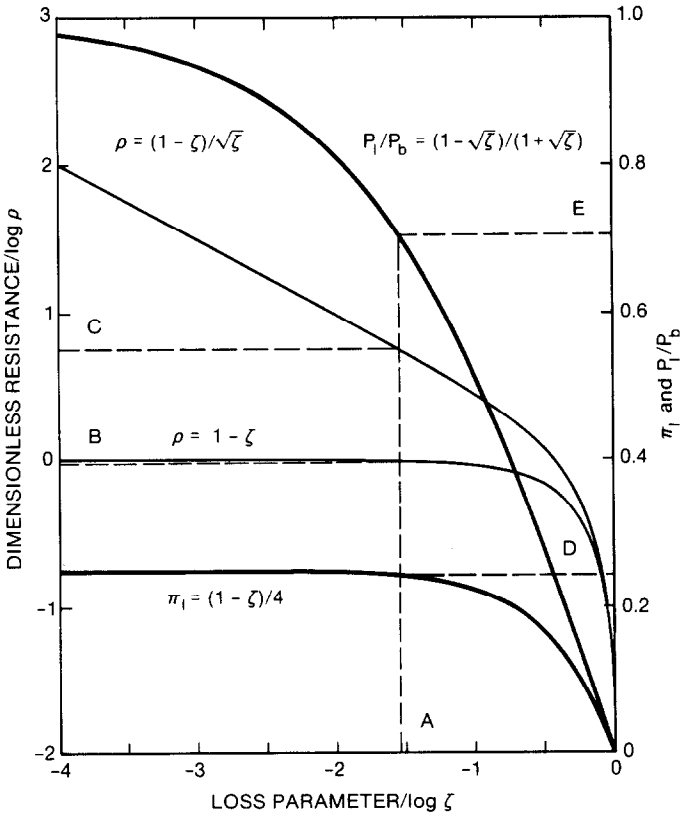

Fig. 7. Plot of design criteria listed in Table 2. Points B, C, D and E are values obtained for the value of ρ indicated by point A. Heavy curves have ordinate scale on the right.

by intercell currents decreases less rapidly than that delivered to the load. Consequently, the design range to trade-off power into load against the material utilized is $1 - \zeta < \rho < (1 - \zeta)\zeta^{-1/2}$. Outside this range both power and stored energy delivered to the load decrease.

The information given in Table 2, and illustrated in Fig. 7, can be used in two ways. First, a range of load resistances can be determined from the knowledge of ζ, *e.g.*, point A; so that at the lower end, *e.g.*, point B, the maximum power is delivered; and at the upper end, *e.g.*, point C, the maximum amount of material is used. These maxima, respectively points D and E, can be found as well. Second, the factor ζ can be designed to provide either a specified maximum power delivery or a specified material utilization. For example, requiring either the maximum power delivery or material use to be greater than that indicated by points D and E, respectively, would limit $\log \zeta$ to be less than the value indicated by point A. Additionally, L_M the relative loss of maximum material use, and L_P the relative loss of power delivery, are listed in Table 2. Evidently, the presence of intercell currents produces a greater relative decrease in material use than in power delivery.

For example, if $\zeta = 0.01$, L_M is 0.18 at maximum material use and 0.02 at maximum power delivery; while L_P, defined only for maximum power delivery, is 0.01.

Conclusions

(i) A simple model devised for the analysis of intercell currents in batteries of pile construction with a common manifold accounts for dissipative losses occurring during discharge and gives their distribution for small intercell currents.

(ii) The initial distribution of dissipative processes is symmetrical. However, in the course of battery discharge, a shift in the distribution occurs. Its magnitude is governed by the charge transfer reactions and the design of manifold.

(iii) Defective cells may create highly localized heat sources which, in turn, may initiate a catastrophic event.

(iv) The use of active material cannot be indefinitely increased by increasing the load resistance, and the relative loss in use of active material exceeds the relative loss in power delivery.

Acknowledgement

This work was supported, in part, by both the Office of Naval Research and the Naval Sea Systems Command and constitutes a fraction of a program to establish a technology base for high discharge rate Li/$SOCl_2$ batteries.

List of symbols

I	Intercell current (A)
J	Loop current (A)
L	Relative loss
N	Number of cells
P	Power (W)
R	Resistance (Ω)
S	Entropy, JK^{-1}
T	Temperature (K)
U	Cell voltage at zero current (V)
V	Cell voltage (V)
w	Cell deficiency factor
α	Index
ζ	Loss parameter
η	Overpotential (V)
λ	Design parameter

Π Dimensionless power
ρ Dimensionless resistance
σ Cell conductivity (S cm^{-2})

Subscripts
a Anodic
b Battery own
c Cathodic
f Manifold feed line
i Running index
k Running index
M Material
n Running index
p Cell port
P Power (W)
l Load
t Manifold tube
z Cell
* Refers to equivalent quantities

References

1 N. D. Koshel and O. S. Ksenzhek, *Elektrokhimiya, 7* (1971) 850.
2 S. Szpak, C. J. Gabriel and J. R. Driscoll, *J. Electrochem. Soc., 131* (1984) 1996.
3 P. van Rysselberghe, *Electrochim. Acta, 11* (1966) 125.
4 P. van Rysselberghe, *Thermodynamics of Irreversible Processes*, Hermann (Paris) and Blaisdell Publ. Co, (New York).
5 S. Szpak, C. J. Gabriel and J. R. Driscoll, *Electrochim. Acta, 32* (1987) 239.